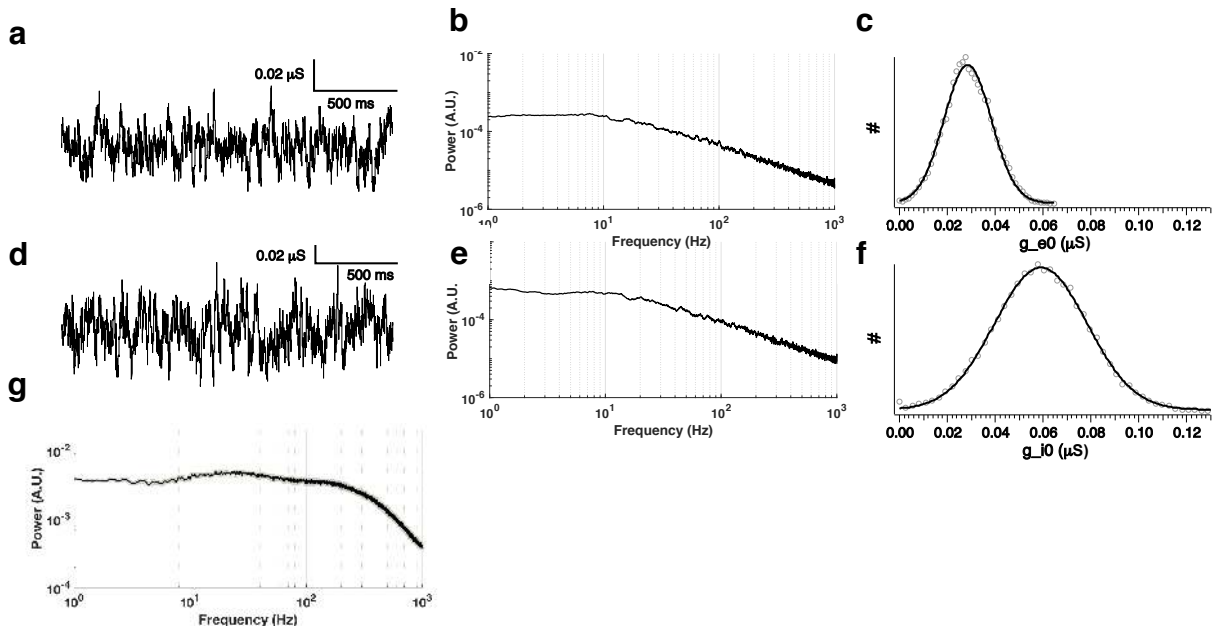# Supplementary information

Theta-resonance and synaptic modulation scale activity patterns in the medial entorhinal cortex stellate cells

Nupur Katyare, Sujit Sikdar (sks@iisc.ac.in)*

Supplementary Figure 1

Supplementary Figure 1 Simulating in-vivo states with the dynamic clamp

a. Stochastic excitatory conductance used for simulating *in-vivo* activity, as a function of time. **b.** power spectrum of the excitatory conductance waveform in a. **c.** histogram of the excitatory conductance waveform in a. **d,e,f.** same as a,b,c for the stochastic inhibitory conductance.

g. Average power spectrum of the resultant injected current (n = 12), error bars are s.e.m.
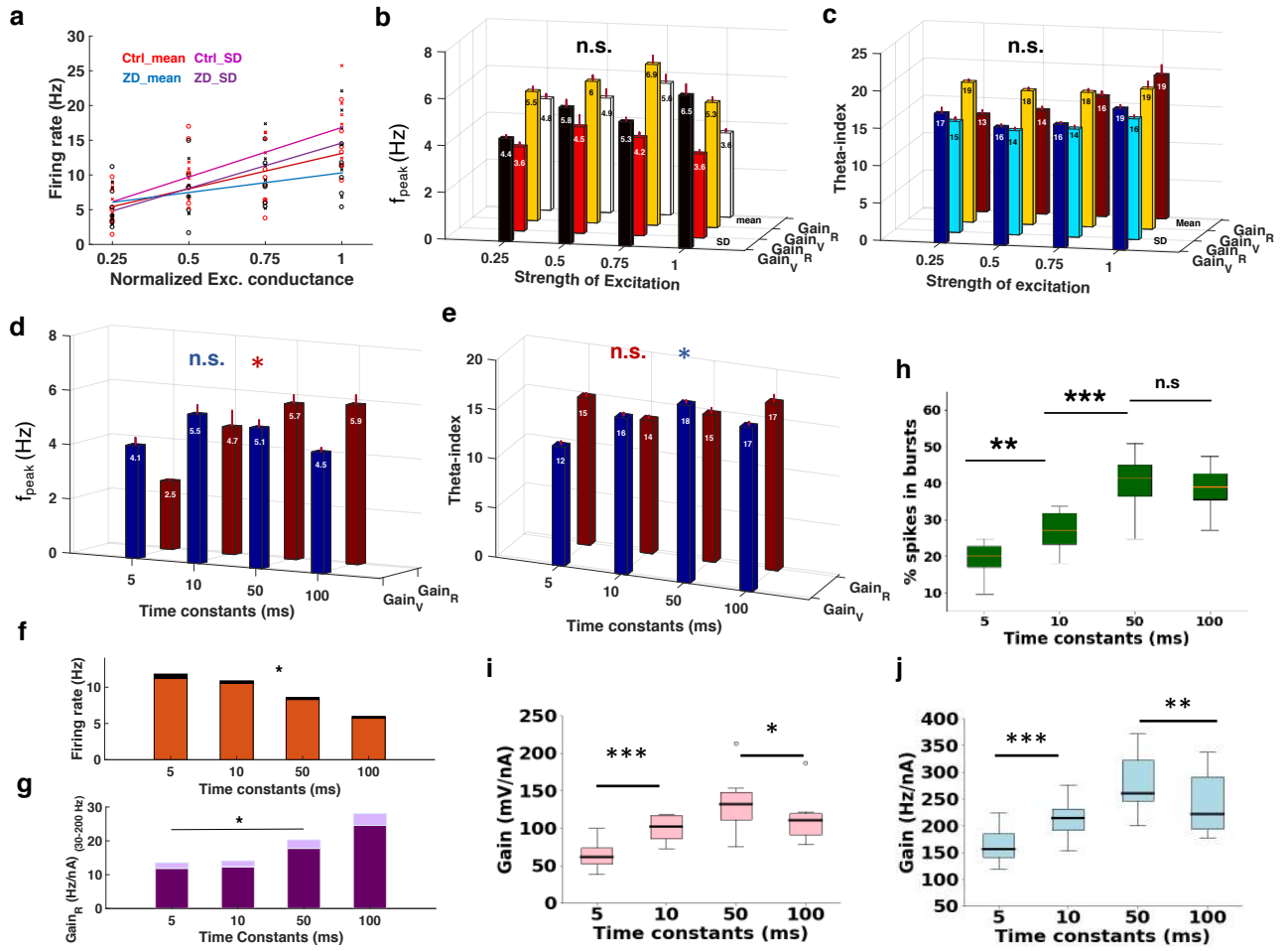
Supplementary Figure 2

a

b

c

d

e

f
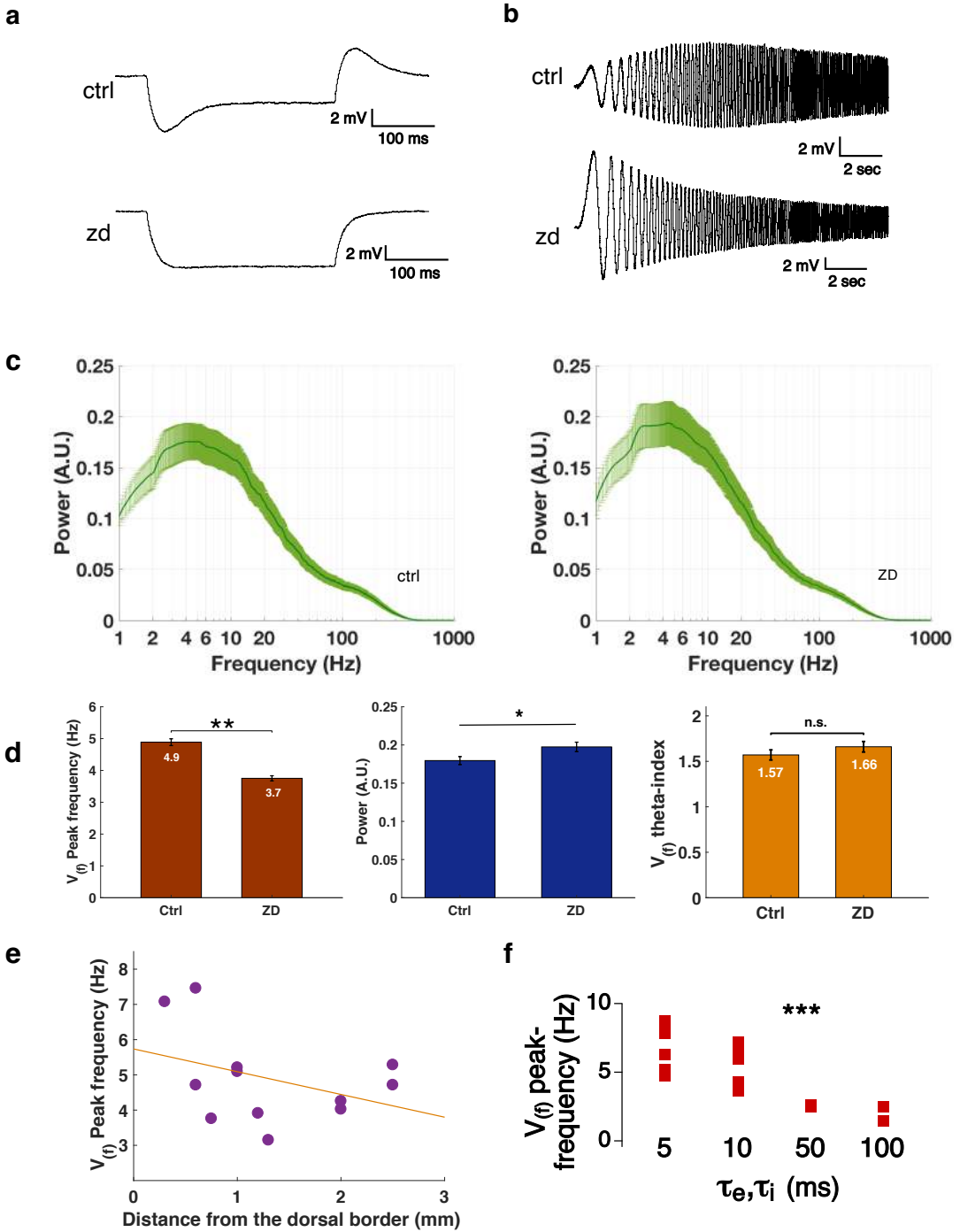
Supplementary figure 2 Analysis of the membrane voltage response under simulated *in-vivo* activity

a. Abolishment of sag in the membrane voltage response in the presence of ZD7288 (ZD) to a -200 pA current stimulus. **b**. Abolishment of theta frequency resonance in membrane voltage response with a 100 pA chirp current stimulus in the presence of ZD7288. **c.** Average power spectrum of the voltage response in control (Left) and after blocking HCN channels with ZD7288 (Right). The plots represent average for 12 cells, error bars are s.e.m. In response to the simulated in-vivo states, we could observe an amplified power in theta frequency (4-14 Hz) in the power spectrum of the membrane voltage response, suggesting a reflection of the theta resonance as observed in the *in-vitro* analyses. Considering the known contribution of the HCN channels, we repeated the measurements after blocking the HCN channels with ZD7288 (ZD), and observed a significant shift of peak in the power spectrum to a lower frequency. **d.** Summary of the changes in the the peak frequency (Left), actual power at peak (Middle) and theta-index (Right) in the presence of ZD7288. **e.** Changes in the peak frequency as a function of D-V distance. The recordings were made from Stellate cells in the parasagittal rat brain slices and most of the cells recorded were from the dorsal part of the medial entorhinal cortex. Within the recorded cells, we could observe the peak of the voltage power spectrum to shift to the lower frequencies in the successive ventral cells. This, along with the differences in the simulation of in-vivo states, could possibly explain the failure of previous studies to observe a similar theta selectivity in the voltage power spectrum (Fernandez & White, 2008). **f.** Changes in the peak frequency as a function of input kinetics. We observed the peak frequency to be sensitive to the synaptic time constants, which could be expected considering the dominance of lower frequencies with the slower synaptic inputs.

d: ** $p < 0.01$, * $p < 0.05$, ; n.s. non-significant, Student's paired t-test, f: *** $p < 0.001$, Kruskal-Wallis test.

Supplementary Figure 3

Supplementary Figure 3 Effect of input statistics on the signal gain

a,b,c. Considering that the input statistics can have a role in determining the actual signal gain (Brunel, Chance, Fourcaud, & Abbott, 2001; Higgs & Spain, 2009), we systematically perturbed the synaptic parameters of the *in-vivo* regime and studied changes in the frequency dependent gain.

To assess the effects of the excitatory drive on the signal gain, we first increased the strength of excitation by increasing the mean (n = 6) and the standard deviation (SD) (n = 9) of the excitatory conductance one at a time. We observed that although the mean firing rate increased linearly with the excitatory strength (a), the fpeak, or the theta-index of GainV or GainR (b,c) did not show any significant change.

d,e. Next, in order to assess the effects of the synaptic kinetics, we repeated the gain measurements while gradually slowing down the kinetics of the excitatory as well as inhibitory conductances (n = 7), by increasing the decay time constants of the synaptic conductances in steps of 5, 10, 50 and 100 ms.

The gainV fpeak was apparently unaffected by the input kinetics (d), however, the theta-index of GainV was observed to increase significantly with the input kinetics (e), possibly, owing to an increased summation of excitatory inputs in the theta frequency. An opposite trend was observed in the case of GainR.

f. Next, analyzing the suprathreshold responses, we observed that the mean firing rate, while still being in theta frequency, decreased significantly as the time constants increased beyond 10 ms, indicating significantly slower rate modulation. **g,h.** Despite the decrease in the mean firing rate, along with the fpeak of GainR (d) the gamma frequency GainR (average gain in 30-200 Hz) (g), showed an interesting overall increase with slower inputs. One of the underlying factors causing this can be the higher frequency bursts, which, apart from increasing the gamma frequency power, when modulated in theta frequency, can give rise to an overall increase in power in theta frequency. To test this, we analyzed the percentage of spikes occurring as bursts (frequency > 50 Hz) for each group, and indeed observed that the bursts increased significantly as the synaptic time constants increased from 5 to 50 ms (h).

i,j. The GainR Gmax, however, similar to GainV Gmax (i) increased up to a certain range (50 ms), and decreased thereafter (j).

These observations are in agreement with the previous findings (Higgs & Spain, 2009), whereby the peak frequency of the lower frequency resonance was observed to increase and the resonance strength was observed to decrease, with an increase in the lower frequency components in the stimulus, mainly as a result of increased propensity of burst firing. Our results thus confirm the role of bursts as a mechanism of active gain modulation.

In summary, on systematically perturbing the synaptic noise statistics, we observed that although the signal gain amplitude was sensitive to the input strength, its frequency selectivity was unaffected by such input scaling.

The differential responsiveness of gain to the mean, SD and kinetics of stimulus can be a dynamic gain control mechanism, wherein the neuronal sensitivity to the input statistics is enhanced, enabling a state-dependent adaptation of their responses. Thus, rather than being dampened by noise, we observed the resonance to instead emerge through the latent noise statistics.

b,c,d,e,f,g: * $p < 0.05$, n.s. non-significant, Kruskal-Wallis test; h,i,j: *** $p < 0.001$, ** $p < 0.01$, * $p < 0.05$, n.s.: non-significant, others: non-significant, Student's paired t-test.
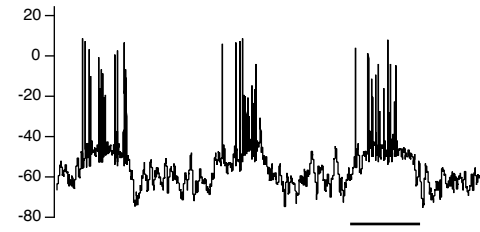
Supplementary Figure 4
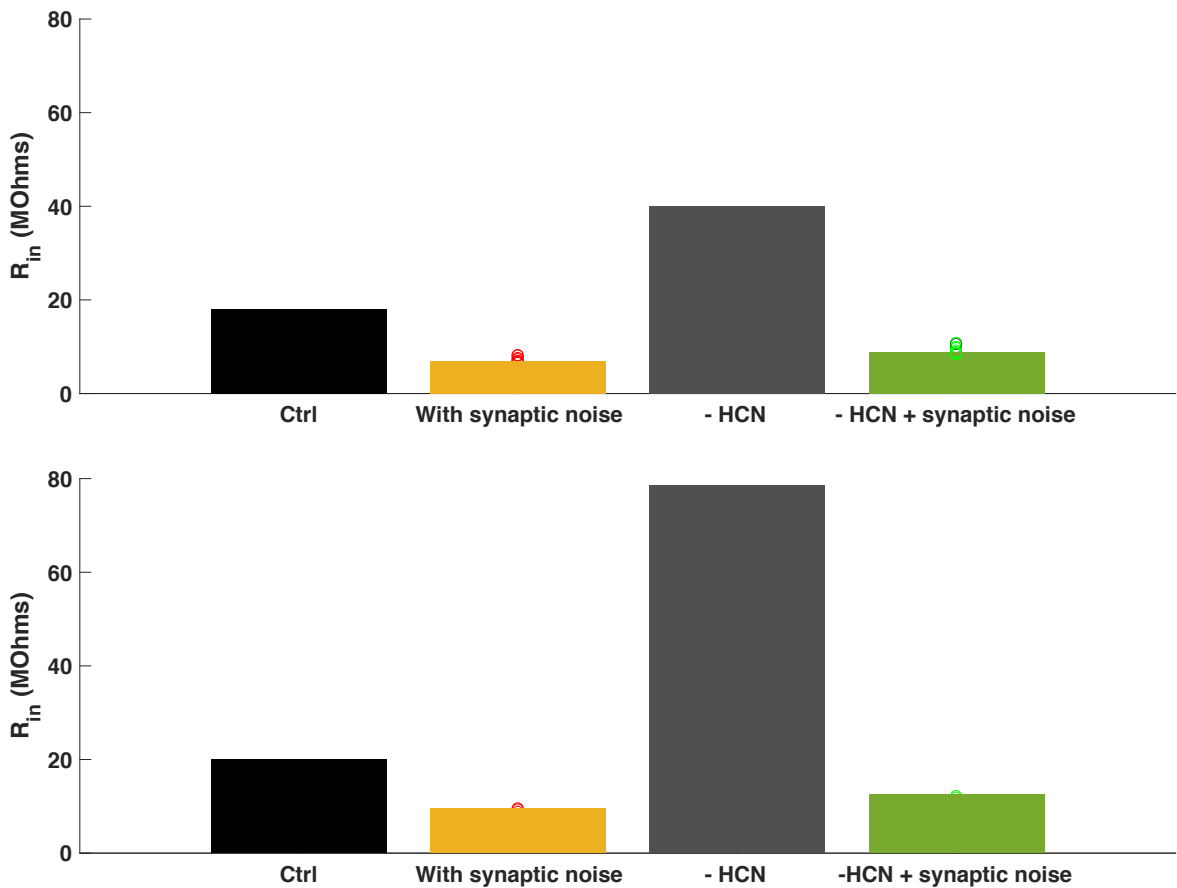
Effects of HCN and background activity on the input resistance.
Input resistance measurements in the computational model (figure 6) at membrane
resistances (R_m) 10000 Ohms (top) and 20000 Ohms (bottom) in the presence and
absence of HCN channels and background synaptic noise as indicated. The data
in the presence of noise represent 10 trials average.

The effects of R_m can be readily observed in the no HCN case, where the input
resistance seems to increase proportionately with R_m. The effects of Rm, however
are less and less pronounced in the presence of HCN and synaptic conductance
noise. It should be noted that the synaptic noise is delivered at the default
conductance parameters used and the effects on input resistance are mainly a
function of the effective strength of excitation and inhibition. Also, with increased
R_m, the integration of synaptic inputs and effective gain can alter. The data thus
indicate that input resistance can be a complex function of many interacting
parameters and can vary drastically depending on the actual behavioral network
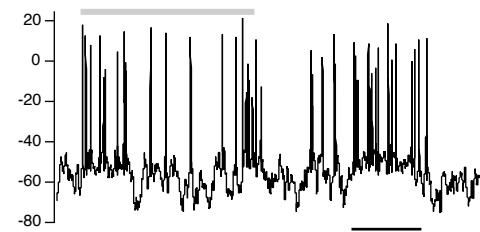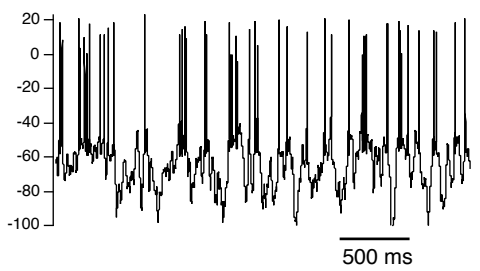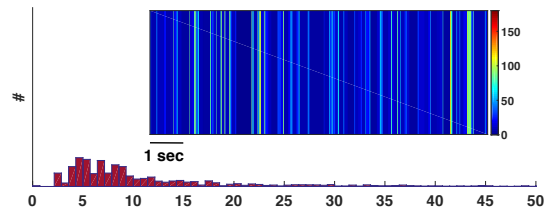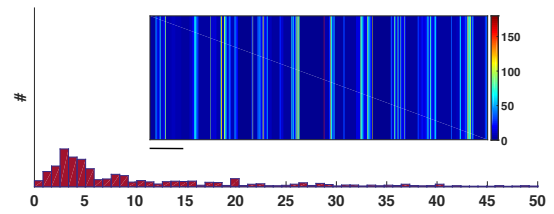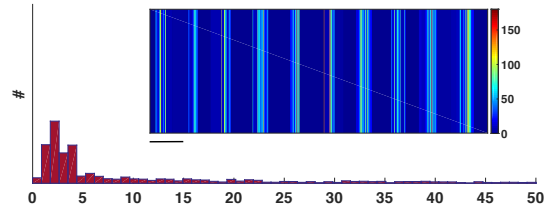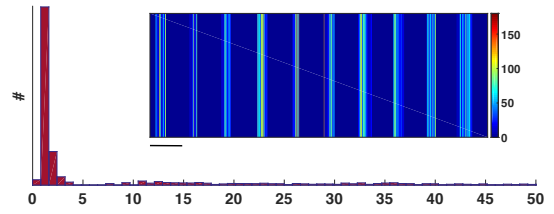states.

Supplementary Figure 5
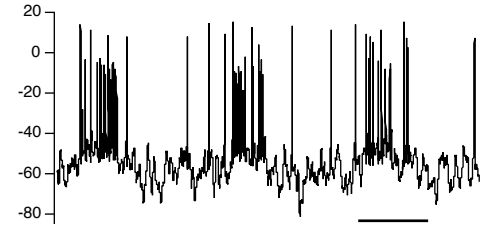
Supplementary Figure 5 Firing patterns in response to a ramp-like excitation

a. Voltage response to a slowly varying (1 Hz) sinusoidal excitatory conductance in the simpler computational model (explained later in this supplementary section), in the presence of the default *in-vivo* like background activity. The default excitatory conductance was reduced to account for the additional excitation. Also, given that no significant difference in the average firing rates of grid cells was observed between the HCN knockout and control animals (Giocomo et al., 2011), the total level of excitation was slightly adjusted so as to match the level of membrane depolarization and average firing rates during different test cases.

 b,c,d Same as a, after reducing HCN conductance to half, removing the HCN conductance, and removing the inhibitory conductance from the model, respectively. **e.** Variations in the instantaneous firing rate over 10 sec. (insets) and histograms of the instantaneous firing rate constructed from 30 sec. long trials of voltage traces in a-d. Color bars represent firing rates in Hz.
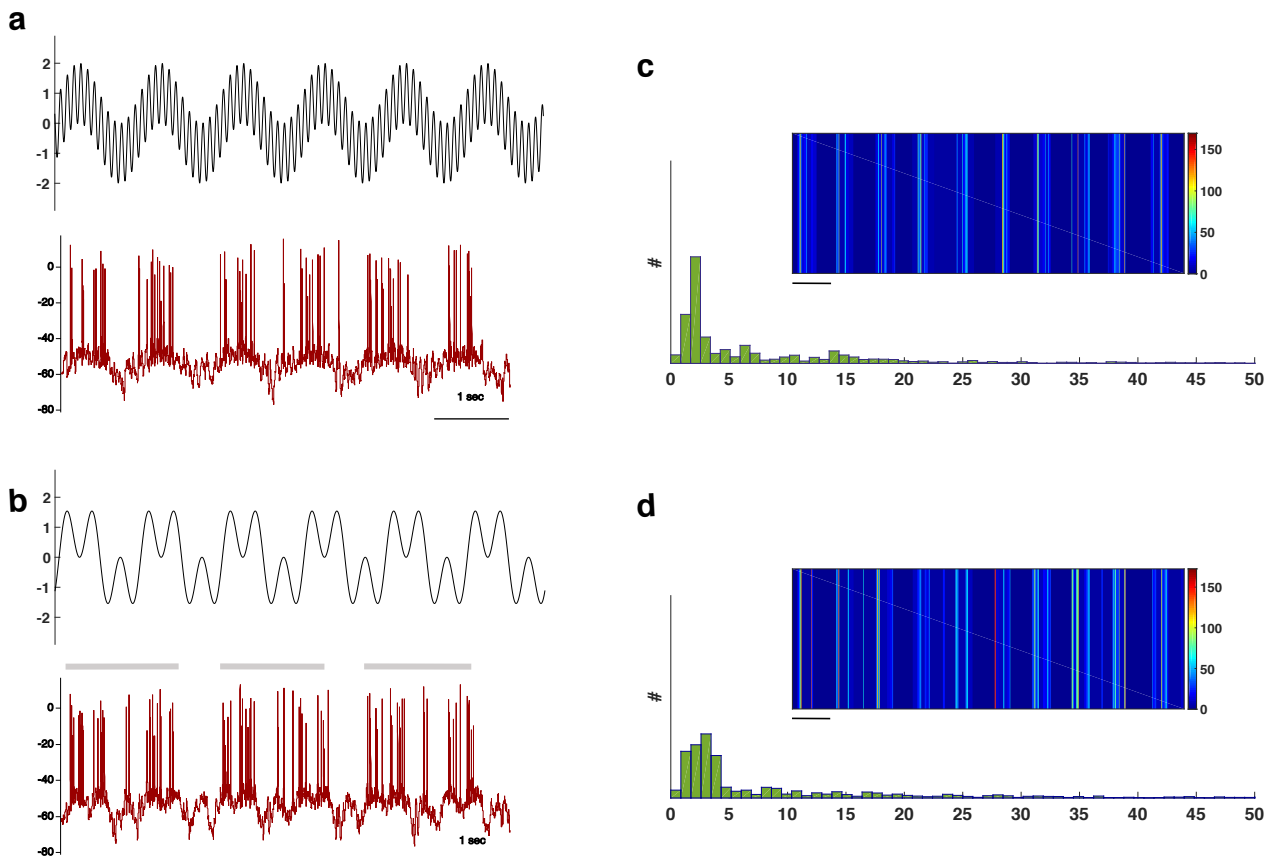
Supplementary Figure 6

Supplementary Figure 6 Interference between the intrinsic rhythm and the periodic synaptic ramps

a. A periodic excitatory conductance mimicking an interference between a 1 Hz and 12 Hz rhythmic activity (top), and the corresponding voltage response (bottom). **b.** A periodic excitatory conductance mimicking an interference between a 1 Hz and 3 Hz rhythmic activity (top), and the corresponding voltage response (bottom). **c,d.** Variations in the instantaneous firing rate over 10 sec. (insets) and histograms of the instantaneous firing rate constructed from 30 sec. long trials of voltage traces in a,b. Color bars represent firing rates in Hz.

Supplementary Figure 6

Interference between the intrinsic rhythm and the periodic synaptic ramps

From the analysis so far, the impact of frequency preferences of Stellate cells in shaping their firing responses was repeatedly revealed, leading us to question whether the same frequency selectivity can underlie the observed firing patterns in response to the ramp like excitation. It has been known that a resonance, when amplified can give rise to an oscillatory activity in the membrane voltage response (Hutcheon & Yarom, 2000) . We have already observed a reflection of the theta frequency resonance in the theta rhythmic modulation of inputs, which gets modulated in lower frequencies in the absence of HCN and inhibition. We have also observed this rhythmic modulation to be strong enough to influence the firing patterns (Fig. 5 & 7). Hence, we questioned whether the observed differences in firing can result from an interaction between the intrinsic rhythmic modulation and the periodic ramps. In the absence of theta activity, the dominant lower frequency modulation of membrane voltage response interacting with the slow ramp-like conductance, can give rise to an interference pattern, whereby the firing patterns are shaped differently, as compared to the interference of the slow ramp-like conductance with the faster theta oscillations. We have illustrated an example of such interactions in Supplementary Fig. 6, where, to test the possibility of such an interaction, we generated a simplified single compartmental neuronal model (details below) and in the presence of in-vivo like activity, subjected it to a periodic excitatory conductance which mimicked an interference between either a 1 Hz and 12 Hz rhythmic activity (Supplementary Fig. 6 a) or between a 1 Hz and 3 Hz rhythmic activity (Supplementary Fig. 6 b). We observed that, in the case of 1 Hz-12 Hz interference, the original 1 Hz period was maintained in the firing patterns (Supplementary Fig. 6 a,c), leading to sharply defined periodic firing fields.

In the 3 Hz case, however, the probability of firing in the troughs of actual 1 Hz conductance was enhanced, owing to a small constructive interference with the 3 Hz rhythmic activity (Supplementary Fig. 6 b,d). As a result, two 1 Hz firing fields were sometimes merged (grey lines in panel b), leading to an increase in the firing period. Despite this, the periodicity was observed to be maintained, possibly owing to the adapting AHP currents, which prevented firing over alternate troughs (Supplementary Fig. 6 b).

Supplementary Figure 4 and 5
Computational model:

A single compartment model was built in NEURON simulation environment (Carnevale & Hines, 2006), with passive and active parameters as follows:

Soma length (μm)	Soma diameter (μm)	R_m ($\Omega.cm^2$)	C_m ($\mu F/cm^2$)	Axial resistance ($\Omega.cm$)
100	100	50000	1	250

The details of the active parameters are discussed below. These were held constant across the models. As the original mechanisms governing the voltage dependence were not tampered, the links to the original .mod mechanism files are provided.

Voltage gated Na+ and K+ channels
From a computational model by (Destexhe *et al.*, 2001).
ModelDB Accession:8115

K$_{AHP}$ channels
From (Migliore, Cook, Jaffe, Turner, & Johnston, 1995).
ModelDB Accession: 3263.

L-type Ca++ channels
Voltage gated high threshold activated calcium channel, from (Migliore et al., 1995).
ModelDB Accession: 3263

Calcium handling mechanism
Models the decay of the internal calcium concentration due to calcium currents and pumps.
From (Destexhe, Contreras, Steriade, Sejnowski, & Huguenard, 1996).
ModelDB Accession: 17663